A STING-CASM-GABARAP Pathway Activates LRRK2 at Lysosomes

Amanda Bentley-DeSousa[1,2,3,4,6] and Shawn M. Ferguson[1,2,3,4,5,6*]

Departments of Cell Biology[1] and Neuroscience[2], Program in Cellular Neuroscience, Neurodegeneration and Repair[3], Wu Tsai Institute[4], Kavli Institute for Neuroscience[5], Yale University School of Medicine, New Haven, Connecticut 06510, USA. Aligning Science Across Parkinson's (ASAP) Collaborative Research Network, Chevy Chase, MD, 20815, USA.[6]

*Correspondence: shawn.ferguson@yale.edu

Running title: CASM-Dependent Activation of LRRK2

Abstract

Mutations that increase LRRK2 kinase activity have been linked to Parkinson's disease and Crohn's disease. LRRK2 is also activated by lysosome damage evoked by chemical and pathogenic stimuli. However, the endogenous cellular mechanisms that control LRRK2 kinase activity are not well understood. In this study, we identify signaling through Stimulator of Interferon Genes (STING) as an upstream activator of LRRK2. This LRRK2 activation occurs via the Conjugation of ATG8 to Single Membranes (CASM) pathway. We furthermore establish that multiple chemical stimuli that perturb lysosomal homeostasis also converge on CASM to activate LRRK2. Although CASM mediates the lipidation of multiple ATG8 protein family members, LRRK2 lysosome recruitment and kinase activation is highly dependent on an interaction with the GABARAP member of this family. Collectively these results define a pathway that integrates multiple stimuli at lysosomes to control the kinase activity of LRRK2. Aberrant activation this pathway may be of relevance in both Parkinson's and Crohn's diseases.

Introduction

Leucine rich repeat kinase 2 (LRRK2) has been linked by human genetics to Parkinson's disease, Crohn's disease and leprosy (Hui et al., 2018; Kalogeropulou et al., 2022; Kluss et al., 2019; Paisan-Ruiz et al., 2004; Rocha et al., 2022; Taylor and Alessi, 2020; Wallings and Tansey, 2019; Zhang et al., 2009; Zhu et al., 2023; Zimprich et al., 2004). LRRK2 mutations cause dominantly inherited familial Parkinson's disease and common variants contribute to sporadic Parkinson's disease risk (Taymans et al., 2023). It is also well established that multiple familial Parkinson's disease LRRK2 missense mutations result in an increase in LRRK2 kinase activity (Kalogeropulou et al., 2022). Conversely, LRRK2 variants associated with decreased risk for Parkinson's and Crohn's disease exhibit reduced kinase activity (Wang et al., 2021). Although mutations that increase LRRK2 activity are only found in a subset of Parkinson's disease patients, this strong link between LRRK activity and Parkinson's disease suggests that LRRK2 functions in a disease relevant pathway and that other factors that modulate LRRK2 kinase activity could have disease relevant consequences. This has stimulated great interest in mechanisms that regulate LRRK2 activity.

Recent studies have converged on endosomes and lysosomes as key intracellular sites of LRRK2 activation. LRRK2 is recruited to lysosomes in response to chemical treatments that impair lysosome function and/or that cause lysosome membrane damage, and this is accompanied by an increase in the kinase activity of LRRK2 (Bonet-Ponce et al., 2020; Eguchi et al., 2018; Herbst et al., 2020; Kalogeropulou et al., 2020; Kluss et al., 2022; Radulovic and Stenmark, 2020). LRRK2 is also activated when pathogens such as *Mycobacterium tuberculosis*, *Listeria monocytogenes* or *Candida albicans* rupture

lysosomes and LRRK2 also participates in a host defense mechanism that is targeted to Salmonella containing vacuoles (Herbst et al., 2020; Lian et al., 2023). The dynamic recruitment of LRRK2 to damaged membranes requires mechanisms whereby endo-lysosome status is sensed and communicated to LRRK2. Understanding the basis for this regulation has implications for understanding both the fundamental cellular functions of LRRK2 and potentially for how LRRK2 is aberrantly activated in disease contexts.

Severely damaged lysosomes are cleared by an autophagic process known as lysophagy wherein they are engulfed and delivered to healthy lysosomes for disposal (Maejima et al., 2013). However, cells can also detect and repair lysosome damage before it reaches the point where lysophagy is required (Bohannon and Hanson, 2020). LRRK2 activation at damaged lysosomes has been proposed to promote the restoration of lysosome integrity by phosphorylating specific Rab GTPases that in turn recruit effectors involved in membrane repair (Bonet-Ponce et al., 2020; Herbst et al., 2020; Steger et al., 2016).

Rab GTPases also act upstream of LRRK2 to promote its membrane recruitment and activation (Dhekne et al., 2023; Eguchi et al., 2018; Gomez et al., 2019; Lian et al., 2023; Pfeffer, 2022; Purlyte et al., 2018; Unapanta et al., 2023; Vides et al., 2022; Wang et al., 2023a). However, although Rab GTPases promote LRRK2 kinase activity in specific contexts, recent knockout mouse studies revealed the persistence of partial or even full LRRK2 kinase activity in multiple tissues even after depletion of key Rab proteins implicated in LRRK2 activation (Dhekne et al., 2023; Kalogeropulou et al., 2020). These results suggest the existence of additional factors that contribute to LRRK2 activation.

Several Parkinson's disease risk genes, including PINK1, Parkin and VPS13C have been linked to the Stimulator of Interferon Genes (STING) signaling pathway that functions as

part of an innate immune response downstream of the sensing of cytoplasmic DNA by cyclic GMP-AMP synthase (cGAS)(Diner et al., 2013; Hancock-Cerutti et al., 2022; Moehlman et al., 2023; Sliter et al., 2018; Wu et al., 2013). Motivated by this convergence of Parkinson's disease genes and the fact that activated STING traffics through cellular compartments (Golgi, Endosomes and Lysosomes) where LRRK2 has been proposed to function, we investigated the relationship between LRRK2 and STING signaling (Erb and Moore, 2020). This led to the discovery of a new pathway wherein STING signals through a process known as Conjugation of ATG8 to Single Membranes (CASM) to activate LRRK2 at lysosomes (Durgan and Florey, 2022). Although CASM results in the lipidation of multiple ATG8 family members, we found that LRRK2 activation is dependent on the GABARAP member of the ATG8 family. This CASM-GABARAP dependent process of LRRK2 activation at lysosomes is required for LRRK2 activation in response to diverse stimuli that perturb the lysosome membrane.

Results

STING is an endogenous activator of LRRK2

Given previously reported links between cGAS-STING dysregulation and Parkinson's disease-associated genes, we sought to test whether STING controls LRRK2 activity. Following treatment of the RAW 264.7 mouse macrophage cell line with STING agonists [2′3′-Cyclic GMP-AMP (cGAMP) and DMXAA (5,6-Dimethylxanthenone-4-acetic Acid)], we observed the expected increases in both STING and TBK1 phosphorylation (Fig. 1A-E). We also measured levels of Rab10 phosphorylation as a readout for changes in LRRK2 kinase activity (Kalogeropulou et al., 2022; Lis et al., 2018; Steger et al., 2016). Activation

of STING by either agonist led to an increase in phosphorylation of Rab10 and the timing of DMXAA-dependent LRRK2 activation also paralleled STING activation (Fig. 1B-E; Fig. S1A). We also assessed Rab12 phosphorylation and found that cGAMP and DMXAA treatments both increased the phosphorylation of this additional LRRK2 substrate (Fig. S1B and C). The absence of Rab10 phosphorylation following STING activation in LRRK2 KO cells demonstrated the essential role for LRRK2 in Rab phosphorylation downstream of STING activation (Fig. 1D). To further test whether these effects were directly due to LRRK2 kinase activity, we acutely treated cells with the LRRK2 inhibitor MLi-2 and found that it also abolished the STING-mediated increase in Rab10 phosphorylation (Fig. 1F). Treating cells with another LRRK2 inhibitor, GZD-824, yielded the same effect (Fig. S1D). We also observed a lack of STING-mediated Rab phosphorylation in cells with a knockin of the inactive LRRK2 T1348N mutant (Ito et al., 2007)(Fig. S1E). Finally, LRRK2 mediated Rab10 phosphorylation following DMXAA treatment occurred with a concentration dependence that paralleled STING activation (Fig. S2A). Altogether, these data demonstrate that STING signaling initiates a response that results in activation of LRRK2 kinase activity.

STING promotes LRRK2 recruitment to lysosomes

Previous studies have shown that upon ligand binding, STING traffics from the endoplasmic reticulum to the Golgi and then to lysosomes where it is internalized and degraded (Balka et al., 2023; Chen et al., 2016; Gonugunta et al., 2017). Consistent with the known requirement for ER to Golgi trafficking as a first step in STING activation, we observed that disruption of such trafficking by treating cells with Brefeldin A prevented STING signaling, as was previously reported (Ishikawa et al., 2009) (Fig. S2B). We also

found that Brefeldin A blocked LRRK2 activation downstream of STING (Fig. S2B). Meanwhile, LRRK2 can be activated at lysosomes in response to various lysosome damaging stimuli (Bonet-Ponce et al., 2020; Eguchi et al., 2018; Herbst et al., 2020; Kalogeropulou et al., 2020). To test the role of lysosomes as sites of STING-dependent LRRK2 activation, we used a previously established method for magnetic isolation of lysosomes from control versus DMXAA stimulated cells that had been pre-loaded with superparamagnetic iron oxide nanoparticles (SPIONs) and found that LRRK2 robustly accumulates on lysosomes in response to STING activation (Amick et al., 2020; Hancock-Cerutti et al., 2022)(Fig. 1G-I).

TBK1 and IKKε are not required for LRRK2 activation by STING

We next implemented a series of genetic perturbations to understand how STING signaling leads to LRRK2 activation. STING KO cells were defective in STING agonist-mediated LRRK2 activation and this was rescued following re-expression of STING (Fig. 2A). Following agonist binding, STING recruits and activates the closely related TBK1 and IKKε kinases (Balka et al., 2020; Chen et al., 2016)(Fig. 1A). Interestingly, TBK1 and IKKε were previously shown to phosphorylate LRRK2 which led us to speculate that this could be part of the pathway whereby STING activates LRRK2 (Dzamko et al., 2012). To test the requirement for TBK1 and IKKε in LRRK2 activation, we generated TBK1 KO, IKKε KO, and TBK1 + IKKε double KO RAW 264.7 cells and measured their ability to activate LRRK2 in response to STING agonist treatment. In each of these KO lines, STING still triggered LRRK2-mediated Rab10 phosphorylation to a degree that was statistically indistinguishable from WT cells (Fig. 2B and C). Furthermore, we still observed LRRK2-mediated Rab10 phosphorylation after rescuing the STING KO cells

with a truncated form of STING (amino acids 1-339) that cannot bind and activate TBK1/IKKε (Gui et al., 2019)(Fig. 2A). These results indicate that STING activates LRRK2 independent of signaling through TBK1 and IKKε kinases.

STING activates LRRK2 via the CASM pathway

In addition to TBK1-IKKε activation, STING also independently activates CASM (also known as V-ATPase–ATG16L1—induced LC3B lipidation or VAIL)(Durgan and Florey, 2022; Fischer et al., 2020; Gui et al., 2019)(Fig. 3A). Consistent with this, we observed that LRRK2 activation by STING ligands was also accompanied by LC3B and GABARAP lipidation (Fig. 3B). ATG16L1 is a scaffold protein that is required for this lipidation reaction (Durgan and Florey, 2022). We therefore generated ATG16L1 KO RAW 264.7 cells, tested their response to STING activation, and found that LRRK2-mediated Rab phosphorylation was abolished (Fig. 3C). This observation led us to focus more deeply on a potential requirement for CASM in LRRK2 activation.

The v-ATPase plays a critical role in the CASM pathway and strategies have been defined that target the v-ATPase to activate or inhibit CASM (Hooper et al., 2022)(Fig. 3A). Saliphenylhalamide (Salip) activates CASM by inhibiting the v-ATPase and stabilizing assembly of the V1 and V0 v-ATPase subunits (Hooper et al., 2022; Xie et al., 2004). Consistent with a role for CASM in activating LRRK2, Salip treatment increased LRRK2-mediated Rab phosphorylation (Fig. 3D and E). In contrast, treatment of cells with folimycin, a v-ATPase inhibitor that binds to a different site than Salip and inhibits CASM (but not the induction of macroautophagy), blocked the activation of LRRK2 downstream of STING (Fig. 3F). Finally, we generated a cell line that stably expresses the Salmonella

effector protein SopF which inhibits CASM by ADP-ribosylating the v-ATPase V_0 subunit (Fischer et al., 2020; Hooper et al., 2022; Xu et al., 2019) and found that this abolished STING-dependent LRRK2 activation (Fig. 3G and H). These tests distinguished between ATG8 family lipidation associated with macroautophagy versus CASM and collectively support an essential role for CASM in mediating LRRK2 activation in response to multiple stimuli.

Multiple chemicals activate LRRK2 via CASM

Multiple chemical stimuli that perturb lysosomes have previously been separately shown to activate LRRK2 and to activate CASM. This includes L-leucyl-L-leucine methyl ester (LLOME), a chemical that selectively damages lysosome membranes following its processing by cathepsin C (Bonet-Ponce et al., 2020; Durgan and Florey, 2022; Kalogeropulou et al., 2020; Thiele and Lipsky, 1990). We confirmed that LLOME activates LRRK2 and established that LLOME also strongly triggers endogenous LRRK2 accumulation on lysosomes in RAW 264.7 cells (Fig. 4A-C). ML SA1 is an activator of the TRPML1 lysosomal cation channel and a known activator of CASM but was not previously shown to activate LRRK2 (Durgan and Florey, 2022; Shen et al., 2012). We found that ML SA1 treatment also activated LRRK2 and that this effect required ATG16L1 (Fig. 4D-F). Nigericin, a proton-potassium ionophore that disrupts ion balances across cellular membranes, is also known to activate both CASM and LRRK2 (Herbst et al., 2020; Hooper et al., 2022; Ito et al., 2016; Jacquin et al., 2017; Kalogeropulou et al., 2020). We confirmed this robust relationship between Nigericin and LRRK2 kinase activity (Fig. 4G). Importantly, the KO of ATG16L1 blocked the ability of Nigericin to activate LRRK2 (Fig.

4H and I). Collectively, these results establish a role for CASM in the activation of LRRK2 by STING as well as by multiple chemical stimuli that perturb lysosomes.

GABARAP is required for CASM-dependent LRRK2 activation

In order define specific cellular machinery that is required for CASM-mediated LRRK2 activation, we performed a targeted siRNA screen focusing on the ATG8-related proteins that are lipidated as part of the CASM pathway. As expected, LRRK2 activity (measured by Rab10 phosphorylation) was reduced by the knockdown of LRRK2 and Rab10 itself as well as by knockdown of Rab12, a recently identified regulator of LRRK2 activity (Dhekne et al., 2023; Wang et al., 2023a)(Fig. 5A). Consistent with a requirement for lipidation of Atg8 family members, depletion of ATG3 and ATG16L1 also reduced the phosphorylation of Rab10 by LRRK2 (Fig. 5A). Interestingly, out of the ATG8 family members annotated in the mouse genome (LC3A, LC3B, Gabarap, GabarapL1, and GabarapL2) only GABARAP was identified as critical for CASM-mediated LRRK2 activation (Fig. 5A). This requirement for GABARAP in LRRK2 activation was independently validated through assays in genome edited GABARAP KO cells where neither DMXAA nor ML SA1 nor Nigericin were able to activate LRRK2 (Fig. 5B-E). Analysis of SPION purified lysosomes furthermore revealed that GABARAP is enriched on lysosomes following STING activation and is required for LRRK2 recruitment to lysosomes (Fig. 5 F and G). Consistent with a direct role for GABARAP in promoting LRRK2 recruitment to lysosomes, HALO-tagged LRRK2 was present in HA-GABARAP immunoprecipitations and this interaction increased in response to STING activation (Fig. 5H and I). Figure S2C shows that the HALO-tagged LRRK2 is functional based on ability to support both basal and DMXAA-stimulated Rab10 phosphorylation when stably

expressed in LRRK2 KO cells. Altogether this data defines a major role for GABARAP in CASM-dependent LRRK2 activation at lysosomes.

Discussion

Collectively, our data defines a pathway for the activation of LRRK2 at lysosomes wherein STING signaling and stimuli that perturb lysosome integrity converge on CASM-mediated GABARAP lipidation to promote LRRK2 lysosome recruitment and activation of LRRK2 kinase activity. Although there has been great progress in elucidating components of the CASM pathway, the physiological functions downstream of CASM have remained elusive (Durgan and Florey, 2022; Hooper et al., 2022; Jacquin et al., 2017; Ulferts et al., 2021; Xu et al., 2019). Our identification of CASM-mediated, GABARAP-dependent, LRRK2 activation provides an important new insight into a functional output of this pathway.

Given that GABARAP lipidation onto intracellular membranes occurs during both conventional macroautophagy and CASM, but only CASM activates LRRK2, an additional factor (or factors) must contribute to the specificity of LRRK2 activation. Candidate contributors to a coincidence detection mechanism to ensure spatial control of LRRK2 activation at GABARAP-positive lysosomes include Rab GTPase proteins that have been demonstrated to mediate LRRK2 membrane recruitment and kinase activation (Pfeffer, 2022). These include Rab10, Rab12 and Rab29 (Dhekne et al., 2023; Purlyte et al., 2018; Vides et al., 2022; Wang et al., 2023a; Zhu et al., 2023). It remains to be determined whether GABARAP acts in parallel with any of these Rabs to ensure that LRRK2 is recruited to and activated at the correct intracellular membranes. It was also very recently

discovered that LRRK2 can assemble into helical polymers on membranes that are enriched in acidic lipid head groups (Wang et al., 2023b). Such LRRK2-membrane interactions could also act together with GABARAP to specify sites of LRRK2 activation.

Although our data is consistent a model (Fig. S3) wherein lipidated GABARAP directly interacts with LRRK2 to help recruit it to lysosomal membranes, our co-immunoprecipitation data does not rule out the possibility that additional proteins are involved in this regulated interaction. Future studies should focus on reconstitution of this interaction with purified proteins and mapping the regions on LRRK2 and GABARAP that mediate their interaction selectively under conditions when GABARAP has been lipidated downstream of CASM.

The importance of LRRK2 kinase activity for Parkinson's disease is well supported by the genetics of both sporadic and familial forms of the disease (Bandres-Ciga et al., 2020; Taylor and Alessi, 2020). The identification of the STING pathway as a robust endogenous activator of LRRK2 suggests that upstream stimuli that activate cGAS-STING may also contribute to Parkinson's disease risk. This includes activation of cGAS in response to release of endogenous DNA from damaged mitochondria and disruptions to nuclear integrity as well as exogenous DNA from pathogen infections (Gulen et al., 2023; Lan et al., 2019; Motwani et al., 2019). Recent findings suggest that in the aging brain such effects are likely to be of particular importance in microglia (Gulen et al., 2023). However, failure of neuronal lysosomes to efficiently degrade nuclear and mitochondrial DNA can also result in STING activation following DNA leakage into the cytoplasm (Lan et al., 2014; Van Acker et al., 2023).

The role for CASM in LRRK2 activation provides a unifying mechanism that explains how diverse stimuli that perturb lysosome integrity and/or ion balance result in LRRK2 activation. In fact, the recent discovery that STING itself is a proton channel suggests that it may activate CASM by disrupting endo-lysosomal pH (Liu et al., 2023). The identification of CASM as a convergence point for multiple stimuli that activate LRRK2 provides a foundation for further investigation of how lysosome dysfunction contributes to Parkinson's disease. CASM-dependent LRRK2 activation may also be relevant for Crohn's disease where human genetics has established roles for both ATG16L1 and LRRK2 and our data now places these genes into a common cellular pathway (Hampe et al., 2007; Van Limbergen et al., 2009).

In conclusion, we have defined a STING-CASM-GABARAP pathway for LRRK2 activation at lysosomes (Fig. S3). This pathway more broadly helps to explain how multiple additional lysosome perturbations activate LRRK2. By establishing a site and machinery for LRRK2 activation, these results provide a new avenue for investigating the regulation of LRRK2 activity in the context of normal physiology as well as human diseases such as Parkinson's disease, Crohn's disease and microbial pathogenesis.

Methods

Cell culture.

RAW 264.7 cells were cultured in DMEM (Thermo Fisher Scientific, 11965-092) + 10% FBS (Thermo Fisher Scientific, 16140-071) + 1% penicillin/streptomycin supplement (Thermo Fisher Scientific, 15140122) at 37°C with 5% CO_2. Details of cell lines are

summarized in Supplemental Table 1. Sources of key reagents are listed in Supplemental Table 2.

Stable Cell Line Generation.

A piggybac transposase strategy was used for stable cell line generation. Briefly, 2.5 x 10^5 cells were plated per well in a 6-well dish. The following day, cells were transfected using Lipofectamine 2000 (Invitrogen, 11668019) or FuGene HD (Promega, E2311), as per the manufacturer's protocols, using a 1:2 ratio of Piggybac transposon plasmid:gene-of-interest plasmid (total 1 ug DNA). After 48 hours, the media was changed. After 72 hours, puromycin (Gibco A11138-03) or blasticidin (Invivogen ant-bl) were used at concentrations of 3.5 µg/mL and 10 µg/mL, respectively. After 48-72 hours, media containing puromycin and blasticidin was washed out with fresh media. After cells had recovered from selection, single cells were plated into 96-well dishes to obtain clonal cell lines. Cell lines were confirmed via immunoblotting. Plasmid information is summarized in Supplemental Table 3.

Custom murine STING, human HALO-LRRK2, and human HA-GABARAP piggybac vectors were purchased from VectorBuilder. The C-terminal truncation of murine STING (to include only amino acids 1-339) was accomplished using NEB Q5 High-Fidelity 2X Master Mix (NEB M0492S) per the manufacturer's protocol. Plasmids were sequenced to confirm successful mutagenesis. pmCherry-SopF was a gift from Leigh Knodler (Addgene plasmid # 135174 ; http://n2t.net/addgene:135174 ; RRID:Addgene_135174)(Lau et al., 2019). In order to create a stable cell line, the mCherry-SopF coding sequence was cloned into the pPB Piggybac plasmid (Vectorbuilder) using the NEB HIFI DNA Assembly Kit (NEB, E2621L).

Genome edited cell lines.

STING KO, TBK1 KO, IKKe KO, TBK1 KO, IKKεε KO, ATG16L1 KO, and GABARAP KO cells were created using the Synthego CRISPR Gene Knockout V2 Mouse Kits for each respective target. Briefly, 2.5 x 10^5 cells were plated into a 6-well dish. The following day, cells were transfected with ribonucleoprotein particles using Lipofectamine CRISPRiMAX (ThermoFisher Scientific, CMAX00003), gene specific sgRNA and recombinant Cas9 (Synthego). After 48 hours, the media was changed. After 72 hours, single cells were plated into 96-well dishes to obtain clonal populations. After expansion of clonal populations, KO clones were identified by immunoblotting.

Generation and use of Superparamagnetic Iron Oxide Nanoparticles (SPIONs).

SPIONS were generated based on an established protocol (Rodriguez-Paris et al., 1993). Briefly, 10 mL of 1.2M $FeCl_2$ (Sigma-Aldrich, 220299) and 10 mL of 1.8M $FeCl_3$ (Sigma-Aldrich, 157740) were combined slowly by stirring. Then, 10 mL of 30% NH_4OH (Sigma-Aldrich, 320145) was slowly added while stirring for 5 minutes. The resulting particles were then washed with 100 mL of water three times. The particles were resuspended in 80 mL of 0.3M HCl (J.T. Baker, 9535) and stirred for 30 minutes. Then, 4g of dextran (Sigma-Aldrich D1662) was added and stirred for 30 minutes. The particles were transferred into dialysis tubing and dialyzed with ddH_2O for at least 2 days with multiple water changes. The particles were centrifuged at 26,900g for 30 minutes to remove large aggregates and stored at 4°C. An established SPION protocol for mouse macrophages was followed for lysosome purification (Rofe and Pryor, 2016) with the exception of using a dounce homogenizer for cell lysis.

Immunoblotting.

1 x 10^6 cells were seeded per well in a 6-well dish. The following day, cells were washed 2 times with ice-cold 1X PBS [1.1 mM KH_2PO_4 (J.T. Baker, 3246-01), 155.2 mM NaCl (Sigma-Aldrich, 3624-05), and 3 mM Na_2HPO_4 (J.T. Baker, 3828-05)] and scraped in 50 µl of ice-cold lysis buffer [50 mM Tris Base (American Bio, AB02000-05000), 150 mM NaCl (Sigma-Aldrich, 3624-05), 1% Triton X-100 (Sigma-Aldrich, X100), 1 mM EDTA (Sigma-Aldrich, 03690) supplemented with cOmplete mini EDTA-free protease inhibitor (Roche, 11836170001) and PhosSTOP (Roche, 4906837001). Lysates were centrifuged at 14,000 RPM (4°C) for 8 minutes to remove insoluble material. Protein concentrations in the supernatants were measured using Coomassie Plus Protein Assay Reagent (ThermoFisher Scientific, 23236) as per manufacturer's protocol. The lysate supernatants were mixed 1:1 with Laemmli Buffer [80 mM Tris-HCl pH 6.8 (American Bio, AB020000-05000 / HCl, Sigma-Aldrich, 3624-06), 25.3% Glycerol (American Bio), 2.67% SDS (American Bioanalytical, AB01920-00500), and Bromphenol Blue (Sigma-Aldrich, B5525) supplemented with 6.187% fresh B-mercaptoethanol (Sigma-Aldrich, M3148)] and heated at 95°C for 3 minutes. Between 20-30 µg of protein was electrophoresed in 4-15% miniPROTEAN TGX Stain-Free pre-cast gels (BioRad, 4568084/4568085/4568086) using electrophoresis buffer [24.76 mM Tris Base (American Bio AB02000-05000), 191.87 mM Glycine (American Bio AB00730-05000), 10 mL 10% SDS (American Bio, AB01920-00500)]. After electrophoresis, gels were transferred onto 0.22 µm pore nitrocellulose membrane (Thermo Fisher Scientific, 1620115) at 100V for 60 minutes in transfer buffer [24.76 mM Tris Base (American Bio AB02000-05000), 191.87 mM Glycine (American Bio AB00730-05000), 20% Methanol (Sigma-Aldrich, 179337-4l-pB)]. Total

protein was visualized using BioRad TGX stain-free technology prior to blocking. Membranes were blocked in 5% non-fat dry milk omniblock (American Bio, AB 10109-01000) in TBST [10 mM Tris Base (American Bio AB02000-05000), 150 mM NaCl (Sigma-Aldrich, 3624-05), 0.1% Tween 20 (Sigma-Aldrich, P7949)]. Antibodies were added in 5% BSA (Sigma-Aldrich, A9647) in TBST overnight (4°C) at the indicated concentrations (supplemental data Table 5). Membranes were washed 2 X 10 minutes with TBST. Secondary was added in TBST or 5% non-fat dry milk Omniblock in TBST (for phospho-specific antibody) at the indicated concentrations for 1 hour at room temperature. Membranes were washed 3 X 10 minutes with TBST. Membranes were subjected to chemiluminescence [SuperSignal West Pico PLUS Chemiluminescence Substrate (Thermo Fisher Scientific, 34580) or SuperSignal West Femto Maximum Sensitivity Substrate (Thermo Fisher Scientific, 34095)] and imaged using a Biorad Chemidoc MP imaging station. A summary of all antibodies used can be found in Table 5 in the supplemental data.,

Immunoprecipitation.

For cell lysis to generate whole cell lysates, the protocol in immunoblotting was followed with few alterations. One 80% confluent 15-cm plate was used per sample. RAW 264.7 LRRK2 KO cells rescued with stably expressed HALO-human LRRK2 (but no HA-GABARAP) were used as a negative control for non-specific LRRK2 interactions with the anti-HA beads. RAW 264.7 LRRK2 KO cells rescued with HALO-LRRK2 and stably expressing HA-tagged human GABARAP were used to test LRRK2-GABARAP interaction. Cells were washed 2X with PBS, scraped in ice-cold lysis buffer, and centrifuged at 14,000 RPM (4°C) for 8 minutes. Protein concentrations were measured

using Coomassie Plus Protein Assay Reagent (ThermoFisher Scientific, 23236) as per manufacturer's protocol. Lysates were then immunoprecipitated using a mix of 15 µl anti-HA beads (Thermo Fisher Scientific, 88837) that were pre-washed 3X with lysis buffer. The same amount of protein was used for each sample. Where needed, samples were supplemented with lysis buffer to maintain the same protein concentration and volume. Lysates were incubated with beads rotating end-over-end for 1 hour at 4°C. Beads were washed 3X with 0.1% TBST and 1X with mq$H_2$0, as per the manufacturer's protocol. Proteins were eluted by incubating beads with Laemmli Buffer and boiling at 95°C for 3 minutes. The sample was then transferred to another microcentrifuge tube and supplemented with 6.187% fresh B-mercaptoethanol (Sigma-Aldrich, M3148). Samples were then subjected to electrophoresis, immunoblotting, and chemiluminescence as previously described above.

siRNA-mediated knockdown.

siRNA knockdowns were accomplished using Horizon Biosciences siGENOME pooled siRNAs. Briefly, 2.5 x 10^5 RAW 264.7 cells were plated per well in a 6-well dish. The following day, cells were transfected using Lipofectamine RNAiMAX (Invitrogen, 2448190) as per the manufacturer's protocols using 100 nM siRNA pool. After 48 hours, cells were treated with drugs or lysed and subjected to immunoblotting. siRNAs used in this study are summarized in Supplemental Table 6.

Statistical analysis.

Statistical analysis was performed with Prism 10 software, with specific details about the statistical tests conducted, the number of independent experiments, and P values provided in the corresponding figure legends.

Acknowledgements

This research was supported by grants from Aligning Science Across Parkinson's disease (ASAP-000580) through the Michael J. Fox Foundation for Parkinson's Research (MJFF) and the Ludwig Foundation. Agnes Roczniak-Ferguson (Yale), Devin Clegg (Yale), Timothy Ryan (Weill-Cornell), Kallol Gupta (Yale) and Pietro De Camilli (Yale) and Tom Melia (Yale) provided valuable feedback. We thank Berrak Ugur (Yale) for managing our ASAP project. The authors do not have any conflicts to declare.

Author contributions

ABD and SMF designed experiments. ABD performed all experiments. ABD and SMF analyzed data and prepared the manuscript.

Figure Legends

Figure 1: STING promotes LRRK2 kinase activity and lysosome recruitment. (A) Schematic representation of STING activation, trafficking and TBK1 activation. (B) Immunoblot analysis displaying the effects of a 2-hour treatment with cGAMP on the indicated proteins in wildtype and LRRK2 knockout cells. (C) Quantification of Rab10 phosphorylation in cGAMP-treated wildtype and LRRK2 knockout cells, with phospho-Rab10 levels normalized to total Rab10. A Two-Tailed Unpaired Welch's t test was performed. P = 0.0118. (D) Immunoblot results demonstrating the impact of a 2-hour treatment with vehicle (DMSO) or DMXAA on the indicated proteins in cells of the specified genotypes. (E) Quantification of Rab10 phosphorylation in DMSO versus

DMXAA-treated cells, with phospho-Rab10 levels normalized to total Rab10. A Two-Tailed Unpaired Welch's t test was performed. P = 0.0163. (F) Immunoblot analysis depicting the effects of a 2-hour treatment with DMXAA on the indicated proteins in cells that were also treated without and with MLi-2. MLi-2 was added 1 hour before the addition of DMXAA and maintained during the DMXAA treatment. (G) Immunoblots of whole cell lysates and SPION-purified lysosomes from cells treated with DMSO or DMXAA for 2 hours. (H) Quantification of LAMP1 enrichment in lysosome versus whole cell lysate (WCL) fractions to demonstrate effective lysosome enrichment. A Two-Tailed Unpaired Welch's t test was performed. P = 0.0140. (I) Quantification of LRRK2 enrichment in the lysosome fractions (normalized to LAMP1 in the same fraction). A Two-Tailed Unpaired Welch's t test was performed. P = 0.0496. Numbers at right of each blot refer to molecular weight (kDa). Error bars represent standard deviations. All experiments were performed in RAW 264.7 cells. Data presented in this figure is representative of results from a minimum of 3 independent experiments.

Figure 2: TBK1 and IKKε are not required for LRRK2 activation by STING. (A) Immunoblots revealing the effects of 2-hour treatments with DMSO or DMXAA on the indicated proteins in wildtype and STING knockout RAW 264.7 cells, along with STING knockout cells that were rescued by stable expression of full-length mouse STING or C-terminally truncated STING (amino acids 1-339). (B) Immunoblot results depicting the effects of 2-hour treatment with vehicle (DMSO) or DMXAA on the indicated proteins in wildtype, TBK1 knockout, IKKε knockout, and TBK1 + IKKε double knockout cells. (C) Quantification of Rab10 phosphorylation in DMSO versus DMXAA-treated cells of the indicated genotypes, with phospho-Rab10 levels normalized to total Rab10. A One-Way

ANOVA was performed. P = 0.9476. Error bars represent standard deviations. Data presented in this figure is representative of results from a minimum of 3 independent experiments. Numbers at right of each blot refer to molecular weight (kDa).

Figure 3: CASM is required for LRRK2 activation by STING. (A) Schematic diagram summarizing the activators and inhibitors of the CASM pathway that were used in experiments in this figure. (B) Immunoblots illustrating the impact of DMXAA treatment on LC3B and GABARAP lipidation in RAW264.7 cells. i = unlipidated, ii = lipidated. (C) Immunoblots displaying the effects of a 2-hour treatment with DMSO versus DMXAA on the indicated proteins in wildtype and ATG16L1 knockout cells. (D) Immunoblot results comparing control versus saliphenylhalimide (Salip) treated cells following a 2-hour treatment. (E) Quantification of the phospho-Rab10/total Rab10 ratio from panel D. A Two-Tailed Unpaired Welch's t test was performed. P = 0.0175. (F) Immunoblots depicting the impact of folimycin (added 1 hour before DMXAA and maintained throughout DMXAA incubation) on the response to a 2-hour treatment with DMSO versus DMXAA on the indicated proteins. (G) Immunoblots from wildtype RAW 264.7 cells versus cells that stably express mCherry-SopF after a 2-hour treatment with DMSO alone versus DMXAA, showing the impact on the indicated proteins in RAW 264.7 cells. (H) Quantification of the phospho-Rab/Rab10 ratios from panel G. A One-Way ANOVA with Sidak's post-test was performed. For WT DMSO vs WT DMXAA, P = 0.0064. For WT DMXAA vs SopF DMXAA, P = 0.0011. Molecular weight markers (kDa) are indicated on the right side of each blot. Error bars represent standard deviations. All experiments were conducted in RAW 264.7 cells, and the data presented in this figure is representative of results obtained from a minimum of three independent experiments.

Figure 4: Multiple stimuli activate LRRK2 through CASM. (A) Immunoblots illustrating the impact of LLOME treatment (2 hours) on phospho-Rab10 and Total Rab10 levels. (B) Immunoblots of whole cell lysates (WCL) and SPION-purified lysosomes from cells treated with LLOME for 2 hours. (C) Quantification of LRRK2 enrichment on lysosomes (normalized to LAMP1) from panel B. A Two-Tailed Unpaired Welch's t test was performed. P = 0.0313. (D) Immunoblots demonstrating the effects of a 2-hour treatment with DMSO versus ML SA1 on Rab10 phosphorylation. (E) Quantification of phospho-Rab10/Rab10 ratios from panel D. A One-Tailed Unpaired Welch's t test was performed. P = 0.0327. (F) Immunoblots showing the effects of a 2-hour treatment with ML SA1 on Phospho-Rab10 and Rab10 in wildtype and ATG16L1 knockout cells. (G) Immunoblots displaying the effects of a 2-hour treatment with Nigericin on Rab10 phosphorylation. (H) Quantification of phospho-Rab10/Rab10 ratios from panel G. A Two-Tailed Unpaired Welch's t test was performed. P = 0.0411. (I) Immunoblots illustrating the effects of a 2-hour treatment with Nigericin on Phospho-Rab10 and Rab10 in wildtype and ATG16L1 knockout cells. Molecular weight markers (kDa) are indicated on the right side of each blot. Error bars represent standard deviations. All experiments were conducted in RAW 264.7 cells, and the data presented in this figure is representative of results obtained from a minimum of three independent experiments.

Figure 5: GABARAP is required for LRRK2 activation and lysosome recruitment. (A) Immunoblot results showing the impact of the indicated siRNAs on Rab10 phosphorylation and additional specified proteins in response to DMXAA. Experiments were performed 48 hours after siRNA transfections. (B) Immunoblots demonstrating the effects of a 2-hour treatment with DMXAA on the indicated proteins in wildtype and

GABARAP knockout cells. (C) Quantification of the phospho-Rab10/Rab10 ratio in panel B. A One-Way ANOVA with Sidak's post-test was performed. For WT DMSO vs WT DMXAA, P = 0.0064. For WT DMXAA vs GABARAP KO DMXAA, P = 0.0011. (D) Immunoblots demonstrating the influence of GABARAP knockout on the phospho-Rab10/Rab10 ratio in response to ML SA1 (2-hour treatment). (E) Immunoblots revealing the effect of GABARAP knockout on the phospho-Rab10/Rab10 ratio in response to Nigericin (2-hour treatment). (F) Immunoblots of whole cell lysates (WCL) and SPION-purified lysosomes from wildtype and GABARAP knockout cells treated with DMSO or DMXAA for 2 hours. (G) Quantification of lysosomal LRRK2 abundance (LRRK2 normalized to LAMP1) from panel F. A One-Way ANOVA with Sidak's post-test was performed. For WT DMSO vs WT DMXAA, P = 0.0002. For WT DMXAA vs GABARAP KO DMXAA, P = 0.0002. (H) Immunoblots of the starting material (Inputs) and anti-HA immunoprecipitates from LRRK2 KO cells that stably express HALO-tagged human LRRK2 +/- HA-tagged human GABARAP, treated for 2 hours with vehicle (DMSO) or DMXAA. (I) Quantification of HALO-LRRK2 abundance in HA-GABARAP immunoprecipitations +/- STING activation with DMXAA. A Two-Tailed Unpaired Welch's t test was performed. P = 0.0243. Molecular weight markers (kDa) are indicated on the right side of each blot. Error bars represent standard deviations. All experiments were conducted in RAW 264.7 cells, and the data presented in this figure is representative of results obtained from a minimum of three independent experiments, except for panel A where n=2.

Summary of Supplemental Material

Figure S1 provides additional evidence in support of STING-dependent activation of LRRK2 kinase activity.

Figure S2 demonstrates concentration dependence of LRRK2 activation, Brefeldin A treatment and HALO-LRRK2 functionality.

Figure S3 contains a schematic diagram that summarizes a STING-CASM-GABARAP pathway for LRRK2 activation at lysosomes.

Supplemental Tables 1-6 provide information concerning reagents and tools used in this study.

References

Amick, J., A.K. Tharkeshwar, G. Talaia, and S.M. Ferguson. 2020. PQLC2 recruits the C9orf72 complex to lysosomes in response to cationic amino acid starvation. *J Cell Biol*. 219.

Balka, K.R., C. Louis, T.L. Saunders, A.M. Smith, D.J. Calleja, D.B. D'Silva, F. Moghaddas, M. Tailler, K.E. Lawlor, Y. Zhan, C.J. Burns, I.P. Wicks, J.J. Miner, B.T. Kile, S.L. Masters, and D. De Nardo. 2020. TBK1 and IKKepsilon Act Redundantly to Mediate STING-Induced NF-kappaB Responses in Myeloid Cells. *Cell Rep*. 31:107492.

Balka, K.R., R. Venkatraman, T.L. Saunders, A. Shoppee, E.S. Pang, Z. Magill, J. Homman-Ludiye, C. Huang, R.M. Lane, H.M. York, P. Tan, R.B. Schittenhelm, S. Arumugam, B.T. Kile, M. O'Keeffe, and D. De Nardo. 2023. Termination of STING responses is mediated via ESCRT-dependent degradation. *EMBO J*. 42:e112712.

Bandres-Ciga, S., M. Diez-Fairen, J.J. Kim, and A.B. Singleton. 2020. Genetics of Parkinson's disease: An introspection of its journey towards precision medicine. *Neurobiol Dis*. 137:104782.

Bohannon, K.P., and P.I. Hanson. 2020. ESCRT puts its thumb on the nanoscale: Fixing tiny holes in endolysosomes. *Curr Opin Cell Biol*. 65:122-130.

Bonet-Ponce, L., A. Beilina, C.D. Williamson, E. Lindberg, J.H. Kluss, S. Saez-Atienzar, N. Landeck, R. Kumaran, A. Mamais, C.K.E. Bleck, Y. Li, and M.R. Cookson. 2020. LRRK2 mediates tubulation and vesicle sorting from lysosomes. *Sci Adv*. 6.

Chen, Q., L. Sun, and Z.J. Chen. 2016. Regulation and function of the cGAS-STING pathway of cytosolic DNA sensing. *Nat Immunol*. 17:1142-1149.

Dhekne, H.S., F. Tonelli, W.M. Yeshaw, C.Y. Chiang, C. Limouse, E. Jaimon, E. Purlyte, D.R. Alessi, and S.R. Pfeffer. 2023. Genome-wide screen reveals Rab12 GTPase as a critical activator of Parkinson's disease-linked LRRK2 kinase. *Elife*. 12.

Diner, E.J., D.L. Burdette, S.C. Wilson, K.M. Monroe, C.A. Kellenberger, M. Hyodo, Y. Hayakawa, M.C. Hammond, and R.E. Vance. 2013. The innate immune DNA sensor cGAS produces a noncanonical cyclic dinucleotide that activates human STING. *Cell Rep*. 3:1355-1361.

Durgan, J., and O. Florey. 2022. Many roads lead to CASM: Diverse stimuli of noncanonical autophagy share a unifying molecular mechanism. *Sci Adv*. 8:eabo1274.

Dzamko, N., F. Inesta-Vaquera, J. Zhang, C. Xie, H. Cai, S. Arthur, L. Tan, H. Choi, N. Gray, P. Cohen, P. Pedrioli, K. Clark, and D.R. Alessi. 2012. The IkappaB kinase

family phosphorylates the Parkinson's disease kinase LRRK2 at Ser935 and Ser910 during Toll-like receptor signaling. *PLoS One*. 7:e39132.

Eguchi, T., T. Kuwahara, M. Sakurai, T. Komori, T. Fujimoto, G. Ito, S.I. Yoshimura, A. Harada, M. Fukuda, M. Koike, and T. Iwatsubo. 2018. LRRK2 and its substrate Rab GTPases are sequentially targeted onto stressed lysosomes and maintain their homeostasis. *Proc Natl Acad Sci U S A*. 115:E9115-E9124.

Erb, M.L., and D.J. Moore. 2020. LRRK2 and the Endolysosomal System in Parkinson's Disease. *J Parkinsons Dis*. 10:1271-1291.

Fischer, T.D., C. Wang, B.S. Padman, M. Lazarou, and R.J. Youle. 2020. STING induces LC3B lipidation onto single-membrane vesicles via the V-ATPase and ATG16L1-WD40 domain. *J Cell Biol*. 219.

Gomez, R.C., P. Wawro, P. Lis, D.R. Alessi, and S.R. Pfeffer. 2019. Membrane association but not identity is required for LRRK2 activation and phosphorylation of Rab GTPases. *J Cell Biol*. 218:4157-4170.

Gonugunta, V.K., T. Sakai, V. Pokatayev, K. Yang, J. Wu, N. Dobbs, and N. Yan. 2017. Trafficking-Mediated STING Degradation Requires Sorting to Acidified Endolysosomes and Can Be Targeted to Enhance Anti-tumor Response. *Cell Rep*. 21:3234-3242.

Gui, X., H. Yang, T. Li, X. Tan, P. Shi, M. Li, F. Du, and Z.J. Chen. 2019. Autophagy induction via STING trafficking is a primordial function of the cGAS pathway. *Nature*. 567:262-266.

Gulen, M.F., N. Samson, A. Keller, M. Schwabenland, C. Liu, S. Gluck, V.V. Thacker, L. Favre, B. Mangeat, L.J. Kroese, P. Krimpenfort, M. Prinz, and A. Ablasser. 2023. cGAS-STING drives ageing-related inflammation and neurodegeneration. *Nature*.

Hampe, J., A. Franke, P. Rosenstiel, A. Till, M. Teuber, K. Huse, M. Albrecht, G. Mayr, F.M. De La Vega, J. Briggs, S. Gunther, N.J. Prescott, C.M. Onnie, R. Hasler, B. Sipos, U.R. Folsch, T. Lengauer, M. Platzer, C.G. Mathew, M. Krawczak, and S. Schreiber. 2007. A genome-wide association scan of nonsynonymous SNPs identifies a susceptibility variant for Crohn disease in ATG16L1. *Nat Genet*. 39:207-211.

Hancock-Cerutti, W., Z. Wu, P. Xu, N. Yadavalli, M. Leonzino, A.K. Tharkeshwar, S.M. Ferguson, G.S. Shadel, and P. De Camilli. 2022. ER-lysosome lipid transfer protein VPS13C/PARK23 prevents aberrant mtDNA-dependent STING signaling. *J Cell Biol*. 221.

Herbst, S., P. Campbell, J. Harvey, E.M. Bernard, V. Papayannopoulos, N.W. Wood, H.R. Morris, and M.G. Gutierrez. 2020. LRRK2 activation controls the repair of damaged endomembranes in macrophages. *EMBO J*. 39:e104494.

Hooper, K.M., E. Jacquin, T. Li, J.M. Goodwin, J.H. Brumell, J. Durgan, and O. Florey. 2022. V-ATPase is a universal regulator of LC3-associated phagocytosis and non-canonical autophagy. *J Cell Biol*. 221.

Hui, K.Y., H. Fernandez-Hernandez, J. Hu, A. Schaffner, N. Pankratz, N.Y. Hsu, L.S. Chuang, S. Carmi, N. Villaverde, X. Li, M. Rivas, A.P. Levine, X. Bao, P.R. Labrias, T. Haritunians, D. Ruane, K. Gettler, E. Chen, D. Li, E.R. Schiff, N. Pontikos, N. Barzilai, S.R. Brant, S. Bressman, A.S. Cheifetz, L.N. Clark, M.J. Daly, R.J.

Desnick, R.H. Duerr, S. Katz, T. Lencz, R.H. Myers, H. Ostrer, L. Ozelius, H. Payami, Y. Peter, J.D. Rioux, A.W. Segal, W.K. Scott, M.S. Silverberg, J.M. Vance, I. Ubarretxena-Belandia, T. Foroud, G. Atzmon, I. Pe'er, Y. Ioannou, D.P.B. McGovern, Z. Yue, E.E. Schadt, J.H. Cho, and I. Peter. 2018. Functional variants in the LRRK2 gene confer shared effects on risk for Crohn's disease and Parkinson's disease. *Sci Transl Med*. 10.

Ishikawa, H., Z. Ma, and G.N. Barber. 2009. STING regulates intracellular DNA-mediated, type I interferon-dependent innate immunity. *Nature*. 461:788-792.

Ito, G., K. Katsemonova, F. Tonelli, P. Lis, M.A. Baptista, N. Shpiro, G. Duddy, S. Wilson, P.W. Ho, S.L. Ho, A.D. Reith, and D.R. Alessi. 2016. Phos-tag analysis of Rab10 phosphorylation by LRRK2: a powerful assay for assessing kinase function and inhibitors. *Biochem J*. 473:2671-2685.

Ito, G., T. Okai, G. Fujino, K. Takeda, H. Ichijo, T. Katada, and T. Iwatsubo. 2007. GTP binding is essential to the protein kinase activity of LRRK2, a causative gene product for familial Parkinson's disease. *Biochemistry*. 46:1380-1388.

Jacquin, E., S. Leclerc-Mercier, C. Judon, E. Blanchard, S. Fraitag, and O. Florey. 2017. Pharmacological modulators of autophagy activate a parallel noncanonical pathway driving unconventional LC3 lipidation. *Autophagy*. 13:854-867.

Kalogeropulou, A.F., J.B. Freemantle, P. Lis, E.G. Vides, N.K. Polinski, and D.R. Alessi. 2020. Endogenous Rab29 does not impact basal or stimulated LRRK2 pathway activity. *Biochem J*. 477:4397-4423.

Kalogeropulou, A.F., E. Purlyte, F. Tonelli, S.M. Lange, M. Wightman, A.R. Prescott, S. Padmanabhan, E. Sammler, and D.R. Alessi. 2022. Impact of 100 LRRK2 variants

linked to Parkinson's disease on kinase activity and microtubule binding. *Biochem J*. 479:1759-1783.

Kluss, J.H., L. Bonet-Ponce, P.A. Lewis, and M.R. Cookson. 2022. Directing LRRK2 to membranes of the endolysosomal pathway triggers RAB phosphorylation and JIP4 recruitment. *Neurobiol Dis*. 170:105769.

Kluss, J.H., A. Mamais, and M.R. Cookson. 2019. LRRK2 links genetic and sporadic Parkinson's disease. *Biochem Soc Trans*. 47:651-661.

Lan, Y.Y., J.M. Heather, T. Eisenhaure, C.S. Garris, D. Lieb, R. Raychowdhury, and N. Hacohen. 2019. Extranuclear DNA accumulates in aged cells and contributes to senescence and inflammation. *Aging Cell*. 18:e12901.

Lan, Y.Y., D. Londono, R. Bouley, M.S. Rooney, and N. Hacohen. 2014. Dnase2a deficiency uncovers lysosomal clearance of damaged nuclear DNA via autophagy. *Cell Rep*. 9:180-192.

Lau, N., A.L. Haeberle, B.J. O'Keeffe, E.A. Latomanski, J. Celli, H.J. Newton, and L.A. Knodler. 2019. SopF, a phosphoinositide binding effector, promotes the stability of the nascent Salmonella-containing vacuole. *PLoS Pathog*. 15:e1007959.

Lian, H., D. Park, M. Chen, F. Schueder, M. Lara-Tejero, J. Liu, and J.E. Galan. 2023. Parkinson's disease kinase LRRK2 coordinates a cell-intrinsic itaconate-dependent defence pathway against intracellular Salmonella. *Nat Microbiol*. 8:1880-1895.

Lis, P., S. Burel, M. Steger, M. Mann, F. Brown, F. Diez, F. Tonelli, J.L. Holton, P.W. Ho, S.L. Ho, M.Y. Chou, N.K. Polinski, T.N. Martinez, P. Davies, and D.R. Alessi. 2018.

Development of phospho-specific Rab protein antibodies to monitor in vivo activity of the LRRK2 Parkinson's disease kinase. *Biochem J*. 475:1-22.

Liu, B., R.J. Carlson, I.S. Pires, M. Gentili, E. Feng, Q. Hellier, M.A. Schwartz, P.C. Blainey, D.J. Irvine, and N. Hacohen. 2023. Human STING is a proton channel. *Science*. 381:508-514.

Maejima, I., A. Takahashi, H. Omori, T. Kimura, Y. Takabatake, T. Saitoh, A. Yamamoto, M. Hamasaki, T. Noda, Y. Isaka, and T. Yoshimori. 2013. Autophagy sequesters damaged lysosomes to control lysosomal biogenesis and kidney injury. *EMBO J*. 32:2336-2347.

Moehlman, A.T., G. Kanfer, and R.J. Youle. 2023. Loss of STING in parkin mutant flies suppresses muscle defects and mitochondria damage. *PLoS Genet*. 19:e1010828.

Motwani, M., S. Pesiridis, and K.A. Fitzgerald. 2019. DNA sensing by the cGAS-STING pathway in health and disease. *Nat Rev Genet*. 20:657-674.

Paisan-Ruiz, C., S. Jain, E.W. Evans, W.P. Gilks, J. Simon, M. van der Brug, A. Lopez de Munain, S. Aparicio, A.M. Gil, N. Khan, J. Johnson, J.R. Martinez, D. Nicholl, I. Marti Carrera, A.S. Pena, R. de Silva, A. Lees, J.F. Marti-Masso, J. Perez-Tur, N.W. Wood, and A.B. Singleton. 2004. Cloning of the gene containing mutations that cause PARK8-linked Parkinson's disease. *Neuron*. 44:595-600.

Pfeffer, S.R. 2022. LRRK2 phosphorylation of Rab GTPases in Parkinson's disease. *FEBS Lett*.

Purlyte, E., H.S. Dhekne, A.R. Sarhan, R. Gomez, P. Lis, M. Wightman, T.N. Martinez, F. Tonelli, S.R. Pfeffer, and D.R. Alessi. 2018. Rab29 activation of the Parkinson's disease-associated LRRK2 kinase. *EMBO J*. 37:1-18.

Radulovic, M., and H. Stenmark. 2020. LRRK2 to the rescue of damaged endomembranes. *EMBO J*. 39:e106162.

Rocha, E.M., M.T. Keeney, R. Di Maio, B.R. De Miranda, and J.T. Greenamyre. 2022. LRRK2 and idiopathic Parkinson's disease. *Trends Neurosci*. 45:224-236.

Rodriguez-Paris, J.M., K.V. Nolta, and T.L. Steck. 1993. Characterization of lysosomes isolated from Dictyostelium discoideum by magnetic fractionation. *J Biol Chem*. 268:9110-9116.

Rofe, A.P., and P.R. Pryor. 2016. Purification of Lysosomes Using Supraparamagnetic Iron Oxide Nanoparticles (SPIONs). *Cold Spring Harb Protoc*. 2016:pdb prot084822.

Shen, D., X. Wang, X. Li, X. Zhang, Z. Yao, S. Dibble, X.P. Dong, T. Yu, A.P. Lieberman, H.D. Showalter, and H. Xu. 2012. Lipid storage disorders block lysosomal trafficking by inhibiting a TRP channel and lysosomal calcium release. *Nat Commun*. 3:731.

Sliter, D.A., J. Martinez, L. Hao, X. Chen, N. Sun, T.D. Fischer, J.L. Burman, Y. Li, Z. Zhang, D.P. Narendra, H. Cai, M. Borsche, C. Klein, and R.J. Youle. 2018. Parkin and PINK1 mitigate STING-induced inflammation. *Nature*. 561:258-262.

Steger, M., F. Tonelli, G. Ito, P. Davies, M. Trost, M. Vetter, S. Wachter, E. Lorentzen, G. Duddy, S. Wilson, M.A. Baptista, B.K. Fiske, M.J. Fell, J.A. Morrow, A.D. Reith,

D.R. Alessi, and M. Mann. 2016. Phosphoproteomics reveals that Parkinson's disease kinase LRRK2 regulates a subset of Rab GTPases. *Elife*. 5.

Taylor, M., and D.R. Alessi. 2020. Advances in elucidating the function of leucine-rich repeat protein kinase-2 in normal cells and Parkinson's disease. *Curr Opin Cell Biol*. 63:102-113.

Taymans, J.M., M. Fell, T. Greenamyre, W.D. Hirst, A. Mamais, S. Padmanabhan, I. Peter, H. Rideout, and A. Thaler. 2023. Perspective on the current state of the LRRK2 field. *NPJ Parkinsons Dis*. 9:104.

Thiele, D.L., and P.E. Lipsky. 1990. Mechanism of L-leucyl-L-leucine methyl ester-mediated killing of cytotoxic lymphocytes: dependence on a lysosomal thiol protease, dipeptidyl peptidase I, that is enriched in these cells. *Proc Natl Acad Sci U S A*. 87:83-87.

Ulferts, R., E. Marcassa, L. Timimi, L.C. Lee, A. Daley, B. Montaner, S.D. Turner, O. Florey, J.K. Baillie, and R. Beale. 2021. Subtractive CRISPR screen identifies the ATG16L1/vacuolar ATPase axis as required for non-canonical LC3 lipidation. *Cell Rep*. 37:109899.

Unapanta, A., F. Shavarebi, J. Porath, Y. Shen, C. Balen, A. Nguyen, J. Tseng, W.S. Leong, M. Liu, P. Lis, S.M. Di Pietro, and A. Hiniker. 2023. Endogenous Rab38 regulates LRRK2's membrane recruitment and substrate Rab phosphorylation in melanocytes. *J Biol Chem*. 299:105192.

Van Acker, Z.P., A. Perdok, R. Hellemans, K. North, I. Vorsters, C. Cappel, J. Dehairs, J.V. Swinnen, R. Sannerud, M. Bretou, M. Damme, and W. Annaert. 2023.

Phospholipase D3 degrades mitochondrial DNA to regulate nucleotide signaling and APP metabolism. *Nat Commun*. 14:2847.

Van Limbergen, J., D.C. Wilson, and J. Satsangi. 2009. The genetics of Crohn's disease. *Annu Rev Genomics Hum Genet*. 10:89-116.

Vides, E.G., A. Adhikari, C.Y. Chiang, P. Lis, E. Purlyte, C. Limouse, J.L. Shumate, E. Spinola-Lasso, H.S. Dhekne, D.R. Alessi, and S.R. Pfeffer. 2022. A feed-forward pathway drives LRRK2 kinase membrane recruitment and activation. *Elife*. 11.

Wallings, R.L., and M.G. Tansey. 2019. LRRK2 regulation of immune-pathways and inflammatory disease. *Biochem Soc Trans*. 47:1581-1595.

Wang, X., V.V. Bondar, O.B. Davis, M.T. Maloney, M. Agam, M.Y. Chin, A. Cheuk-Nga Ho, R. Ghosh, D.E. Leto, D. Joy, M.E.K. Calvert, J.W. Lewcock, G. Di Paolo, R.G. Thorne, Z.K. Sweeney, and A.G. Henry. 2023a. Rab12 is a regulator of LRRK2 and its activation by damaged lysosomes. *Elife*. 12.

Wang, X., J. Espadas, Y. Wu, S. Cai, J. Ge, L. Shao, A. Roux, and P. De Camilli. 2023b. Membrane remodeling properties of the Parkinson's disease protein LRRK2. *Proc Natl Acad Sci U S A*. 120:e2309698120.

Wang, X., E. Negrou, M.T. Maloney, V.V. Bondar, S.V. Andrews, M. Montalban, C. Llapashtica, R. Maciuca, H. Nguyen, H. Solanoy, A. Arguello, L. Przybyla, N.J. Moerke, S. Huntwork-Rodriguez, and A.G. Henry. 2021. Understanding LRRK2 kinase activity in preclinical models and human subjects through quantitative analysis of LRRK2 and pT73 Rab10. *Sci Rep*. 11:12900.

Wu, J., L. Sun, X. Chen, F. Du, H. Shi, C. Chen, and Z.J. Chen. 2013. Cyclic GMP-AMP is an endogenous second messenger in innate immune signaling by cytosolic DNA. *Science*. 339:826-830.

Xie, X.S., D. Padron, X. Liao, J. Wang, M.G. Roth, and J.K. De Brabander. 2004. Salicylihalamide A inhibits the V0 sector of the V-ATPase through a mechanism distinct from bafilomycin A1. *J Biol Chem*. 279:19755-19763.

Xu, Y., P. Zhou, S. Cheng, Q. Lu, K. Nowak, A.K. Hopp, L. Li, X. Shi, Z. Zhou, W. Gao, D. Li, H. He, X. Liu, J. Ding, M.O. Hottiger, and F. Shao. 2019. A Bacterial Effector Reveals the V-ATPase-ATG16L1 Axis that Initiates Xenophagy. *Cell*. 178:552-566 e520.

Zhang, F.R., W. Huang, S.M. Chen, L.D. Sun, H. Liu, Y. Li, Y. Cui, X.X. Yan, H.T. Yang, R.D. Yang, T.S. Chu, C. Zhang, L. Zhang, J.W. Han, G.Q. Yu, C. Quan, Y.X. Yu, Z. Zhang, B.Q. Shi, L.H. Zhang, H. Cheng, C.Y. Wang, Y. Lin, H.F. Zheng, X.A. Fu, X.B. Zuo, Q. Wang, H. Long, Y.P. Sun, Y.L. Cheng, H.Q. Tian, F.S. Zhou, H.X. Liu, W.S. Lu, S.M. He, W.L. Du, M. Shen, Q.Y. Jin, Y. Wang, H.Q. Low, T. Erwin, N.H. Yang, J.Y. Li, X. Zhao, Y.L. Jiao, L.G. Mao, G. Yin, Z.X. Jiang, X.D. Wang, J.P. Yu, Z.H. Hu, C.H. Gong, Y.Q. Liu, R.Y. Liu, D.M. Wang, D. Wei, J.X. Liu, W.K. Cao, H.Z. Cao, Y.P. Li, W.G. Yan, S.Y. Wei, K.J. Wang, M.L. Hibberd, S. Yang, X.J. Zhang, and J.J. Liu. 2009. Genomewide association study of leprosy. *N Engl J Med*. 361:2609-2618.

Zhu, C., S. Herbst, and P.A. Lewis. 2023. Leucine-rich repeat kinase 2 at a glance. *J Cell Sci*. 136.

Zimprich, A., S. Biskup, P. Leitner, P. Lichtner, M. Farrer, S. Lincoln, J. Kachergus, M. Hulihan, R.J. Uitti, D.B. Calne, A.J. Stoessl, R.F. Pfeiffer, N. Patenge, I.C. Carbajal, P. Vieregge, F. Asmus, B. Muller-Myhsok, D.W. Dickson, T. Meitinger, T.M. Strom, Z.K. Wszolek, and T. Gasser. 2004. Mutations in LRRK2 cause autosomal-dominant parkinsonism with pleomorphic pathology. *Neuron*. 44:601-607.

Figure 1

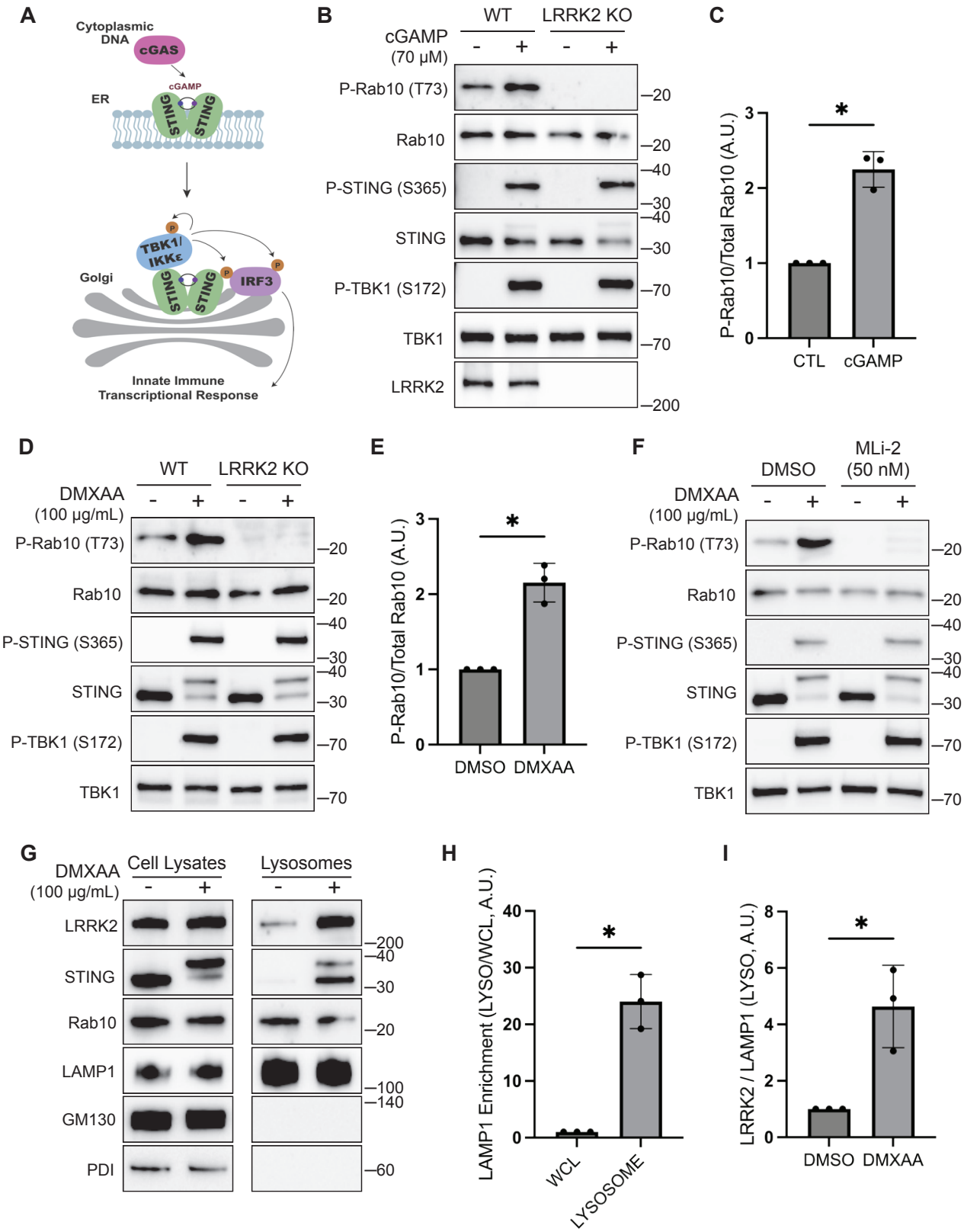
A
Cytoplasmic DNA
cGAS
cGAMP
ER
STING
STING
TBK1/ IKKε
IRF3
Golgi
Innate Immune Transcriptional Response
B
WT
LRRK2 KO
cGAMP (70 μM)
- + - +
P-Rab10 (T73)
Rab10
P-STING (S365)
STING
P-TBK1 (S172)
TBK1
LRRK2
20
20
40
30
40
30
70
70
200
C
P-Rab10/Total Rab10 (A.U.)
CTL
cGAMP
D
WT
LRRK2 KO
DMXAA (100 μg/mL)
- + - +
P-Rab10 (T73)
Rab10
P-STING (S365)
STING
P-TBK1 (S172)
TBK1
E
P-Rab10/Total Rab10 (A.U.)
DMSO
DMXAA
F
DMSO
MLi-2 (50 nM)
DMXAA (100 μg/mL)
- + - +
P-Rab10 (T73)
Rab10
P-STING (S365)
STING
P-TBK1 (S172)
TBK1
G
DMXAA (100 μg/mL)
Cell Lysates
Lysosomes
- + - +
LRRK2
STING
Rab10
LAMP1
GM130
PDI
200
40
30
20
100
140
60
H
LAMP1 Enrichment (LYSO/WCL, A.U.)
WCL
LYSOSOME
I
LRRK2 / LAMP1 (LYSO, A.U.)
DMSO
DMXAA

Figure 2

A

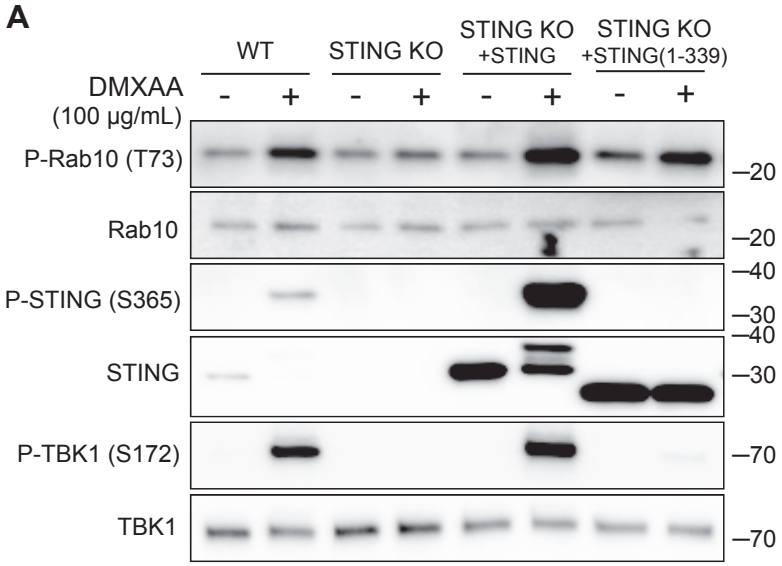
WT
STING KO
STING KO +STING
STING KO +STING(1-339)
DMXAA (100 μg/mL)
- + - + - + - +
P-Rab10 (T73)
Rab10
P-STING (S365)
STING
P-TBK1 (S172)
TBK1
–20
–20
–40
–30
–40
–30
–70
–70

B

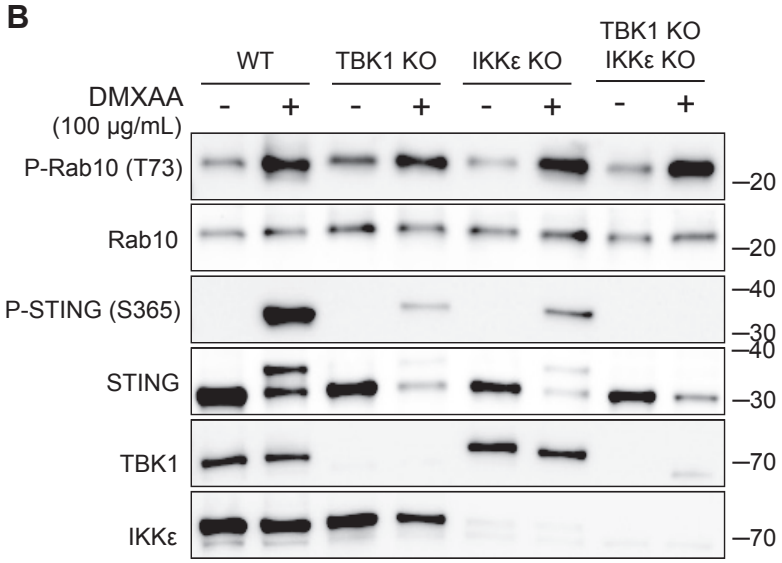
WT
TBK1 KO
IKKε KO
TBK1 KO IKKε KO
DMXAA (100 μg/mL)
- + - + - + - +
P-Rab10 (T73)
Rab10
P-STING (S365)
STING
TBK1
IKKε
–20
–20
–40
–30
–40
–30
–70
–70

C

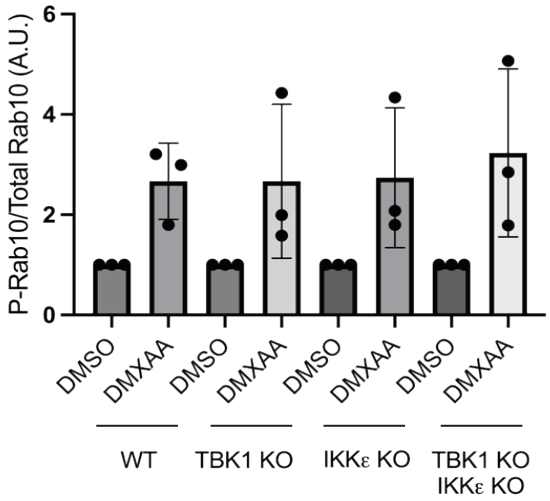
P-Rab10/Total Rab10 (A.U.)
0
2
4
6
DMSO
DMXAA
DMSO
DMXAA
DMSO
DMXAA
DMSO
DMXAA
WT
TBK1 KO
IKKε KO
TBK1 KO IKKε KO

Figure 3

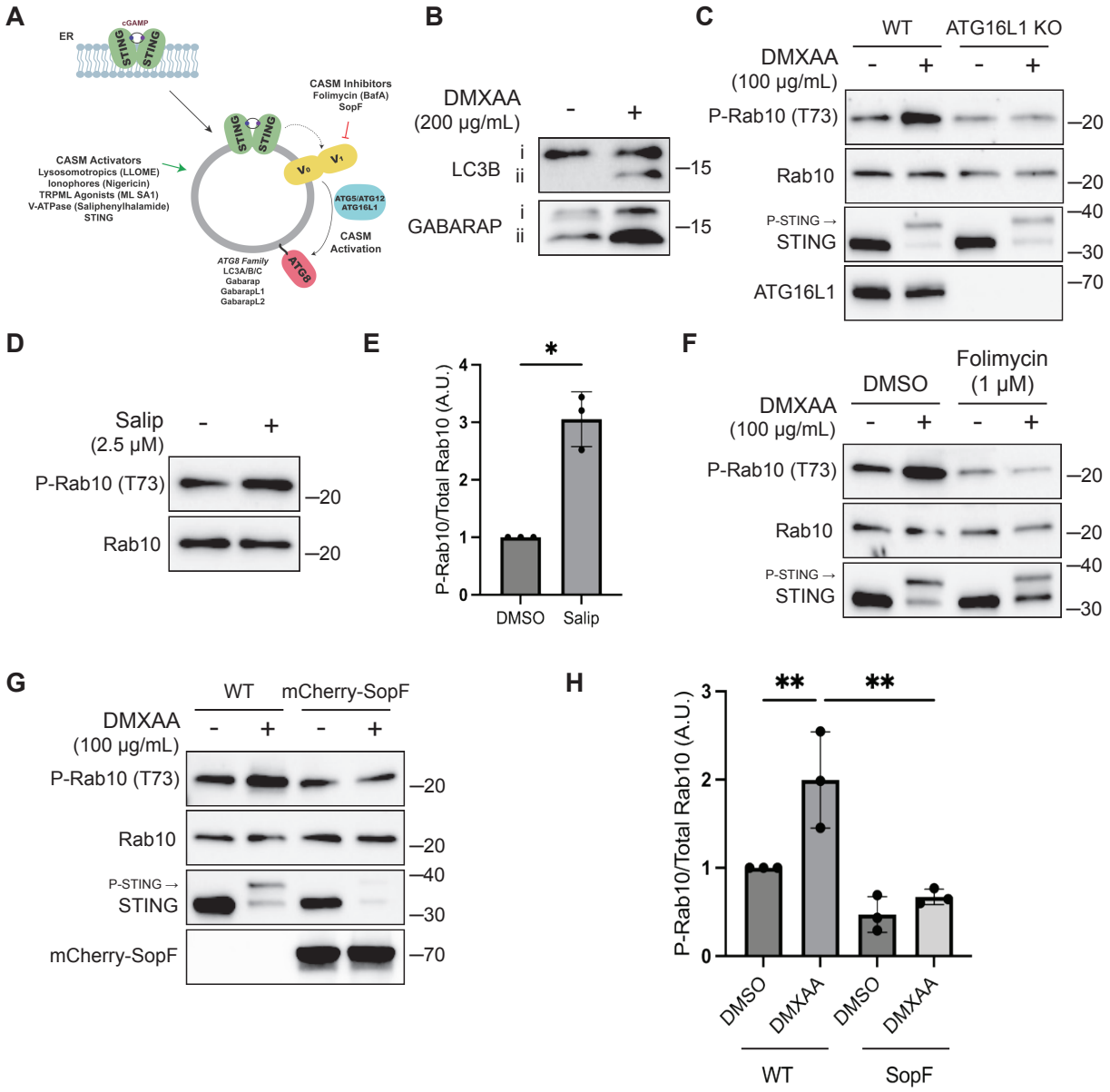
A
ER
cGAMP
STING
STING
CASM Inhibitors
Folimycin (BafA)
SopF
CASM Activators
Lysosomotropics (LLOME)
Ionophores (Nigericin)
TRPML Agonists (ML SA1)
V-ATPase (Saliphenylhalamide)
STING
V0
V1
ATG5/ATG12
ATG16L1
CASM
Activation
ATG8 Family
LC3A/B/C
Gabarap
GabarapL1
GabarapL2
ATG8
B
DMXAA
(200 μg/mL)
-
+
LC3B
i
ii
GABARAP
i
ii
–15
–15
C
WT
ATG16L1 KO
DMXAA
(100 μg/mL)
- + - +
P-Rab10 (T73)
Rab10
P-STING →
STING
ATG16L1
–20
–20
–40
–30
–70
D
Salip
(2.5 μM)
- +
P-Rab10 (T73)
Rab10
–20
–20
E
P-Rab10/Total Rab10 (A.U.)
0
1
2
3
4
*
DMSO
Salip
F
DMSO
Folimycin
(1 μM)
DMXAA
(100 μg/mL)
- + - +
P-Rab10 (T73)
Rab10
P-STING →
STING
–20
–20
–40
–30
G
WT
mCherry-SopF
DMXAA
(100 μg/mL)
- + - +
P-Rab10 (T73)
Rab10
P-STING →
STING
mCherry-SopF
–20
–20
–40
–30
–70
H
P-Rab10/Total Rab10 (A.U.)
0
1
2
3
**
**
DMSO
DMXAA
DMSO
DMXAA
WT
SopF

Figure 4

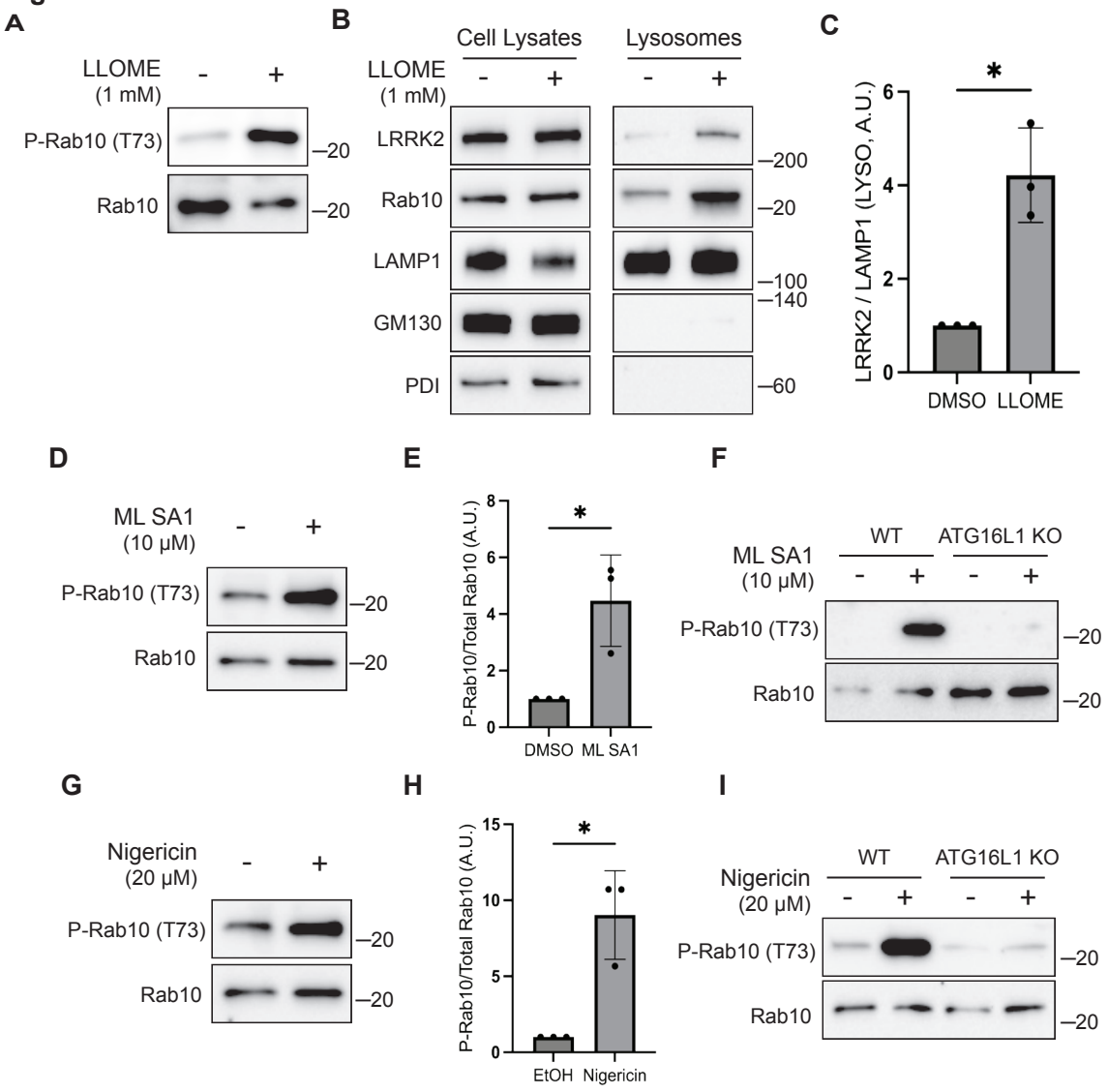
A
LLOME (1 mM)
-
+
P-Rab10 (T73)
Rab10
–20
–20
B
Cell Lysates
Lysosomes
LLOME (1 mM)
-
+
-
+
LRRK2
Rab10
LAMP1
GM130
PDI
–200
–20
–100
–140
–60
C
*
LRRK2 / LAMP1 (LYSO, A.U.)
0
2
4
6
DMSO
LLOME
D
ML SA1 (10 μM)
-
+
P-Rab10 (T73)
Rab10
–20
–20
E
*
P-Rab10/Total Rab10 (A.U.)
0
2
4
6
8
DMSO
ML SA1
F
WT
ATG16L1 KO
ML SA1 (10 μM)
-
+
-
+
P-Rab10 (T73)
Rab10
–20
–20
G
Nigericin (20 μM)
-
+
P-Rab10 (T73)
Rab10
–20
–20
H
*
P-Rab10/Total Rab10 (A.U.)
0
5
10
15
EtOH
Nigericin
I
WT
ATG16L1 KO
Nigericin (20 μM)
-
+
-
+
P-Rab10 (T73)
Rab10
–20
–20

Figure 5

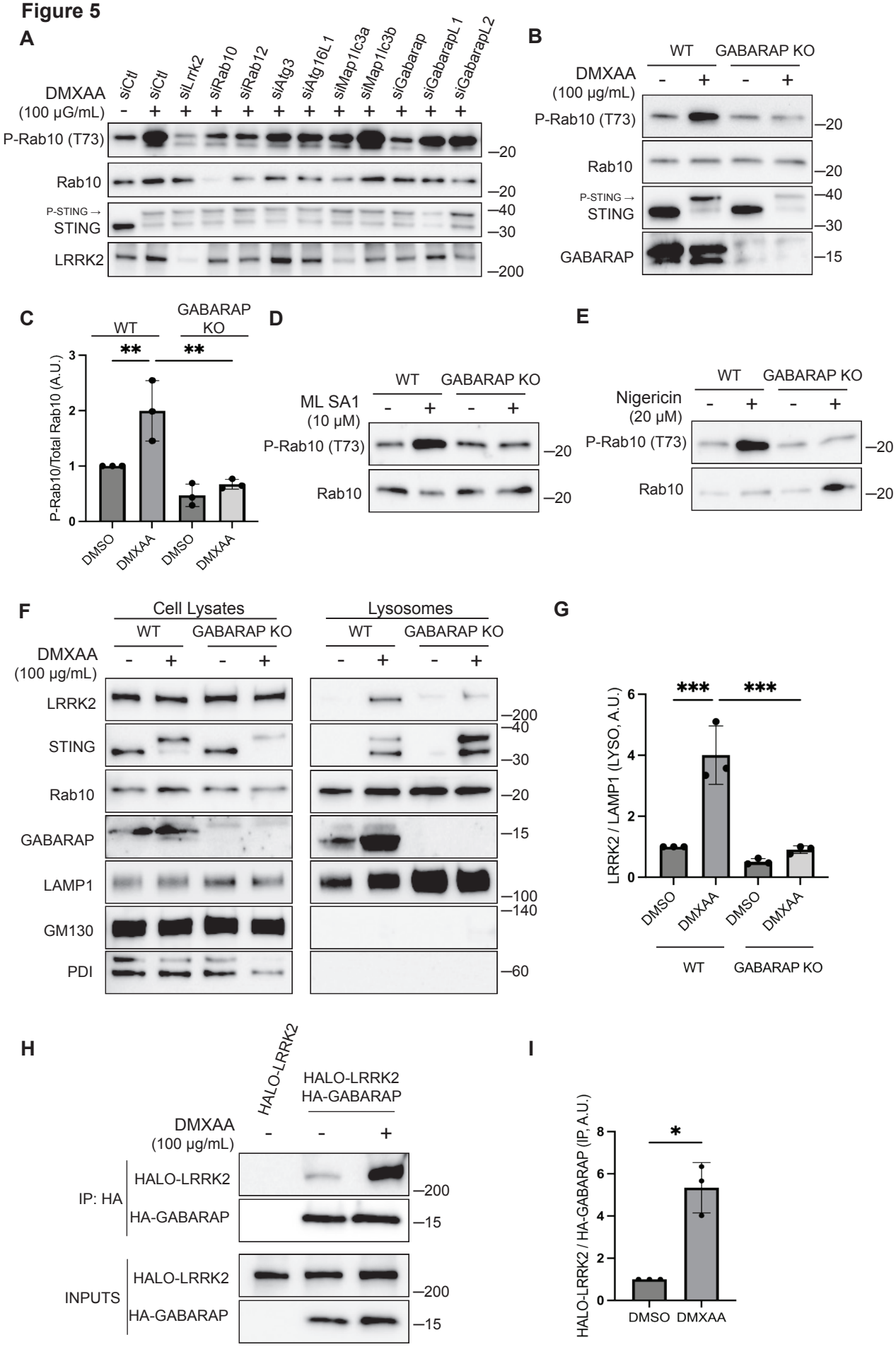
A
siCtl
siCtl
siLrrk2
siRab10
siRab12
siAtg3
siAtg16L1
siMap1lc3a
siMap1lc3b
siGabarap
siGabarapL1
siGabarapL2
DMXAA (100 µG/mL)
P-Rab10 (T73)
Rab10
P-STING →
STING
LRRK2
–20
–20
–40
–30
–200
B
WT
GABARAP KO
DMXAA (100 µg/mL)
P-Rab10 (T73)
Rab10
P-STING →
STING
GABARAP
–20
–20
–40
–30
–15
C
WT
GABARAP KO
P-Rab10/Total Rab10 (A.U.)
DMSO
DMXAA
DMSO
DMXAA
D
WT
GABARAP KO
ML SA1 (10 µM)
P-Rab10 (T73)
Rab10
–20
–20
E
WT
GABARAP KO
Nigericin (20 µM)
P-Rab10 (T73)
Rab10
–20
–20
F
Cell Lysates
Lysosomes
WT
GABARAP KO
DMXAA (100 µg/mL)
LRRK2
STING
Rab10
GABARAP
LAMP1
GM130
PDI
–200
–40
–30
–20
–15
–100
–140
–60
G
LRRK2 / LAMP1 (LYSO, A.U.)
DMSO
DMXAA
DMSO
DMXAA
WT
GABARAP KO
H
HALO-LRRK2
HALO-LRRK2
HA-GABARAP
DMXAA (100 µg/mL)
IP: HA
HALO-LRRK2
HA-GABARAP
INPUTS
HALO-LRRK2
HA-GABARAP
–200
–15
–200
–15
I
HALO-LRRK2 / HA-GABARAP (IP, A.U.)
DMSO
DMXAA